Cell Biology and Toxicology. 1994; **10**: 207–218.

Different susceptibilities to cell death induced by t-butylhydroperoxide could depend upon cell histotype-associated growth features

W. Malorni, G. Rainaldi, R. Rivabene and M.T. Santini
Department of Ultrastructures, Istituto Superiore di Sanità, Viale Regina Elena 299, 00161 Rome, Italy

Received 3 February 1994; accepted 25 July 1994

Keywords: blebbing, cell death, cytoskeleton, mitochondria, oxidative stress, t-BHP

Abstract

The effects of the oxidizing agent t-butylhydroperoxide (t-BHP) were investigated on three human cell lines of different origin and growth features (A431 epithelial cells, ADF astrocytoma cells and U937 leukemic cells) using electron microscopy and electron paramagnetic resonance spectroscopy. The results indicate that important biophysical and ultrastructural modifications are induced in the plasma and mitochondrial membranes of these cells and that these changes can ultimately lead to cell death. In addition, the cell cytoskeleton also appears to be a target of hydroperoxide-mediated stress. In particular, all three cell types undergo cytoskeletal alterations leading to surface blebbing, a typical characteristic of cell damage. However, the timing and extent of this damage as well as that occurring at the mitochondrial and plasma membrane levels seems to be different: cells with weak (ADF) or absent (U937) cell-to-cell and cell–substrate contacts and a poorly developed cytoskeleton appear to be more susceptible than other cell types (e.g., A431) to t-BHP-mediated injury. These diverse cell susceptibilities to hydroperoxide-mediated oxidative stress could thus depend upon cell histotype-associated growth featurs.

Abbreviations: t-BHP, tert-butylhydroperoxide; DMEM, Dulbecco's Modified Eagle's Medium; EPR, electron paramagnetic resonance; GSH, reduced glutathione; 5-NSA, nitroxystearic acid; PBS, phosphate-buffered saline

Introduction

Oxidative damage to cells appears to have a role in many pathological conditions and disorders including carcinogenesis and aging (Gutteridge, 1993). The formation of reactive oxygen species and free radicals has in fact been implicated in numerous deleterious processes, including lipid peroxidation, modification of organelle integrity and function, ion deregulation, and damage to DNA (Sies, 1985, 1991). The complex cascade of subcellular events initiated by oxidative damage can impair normal cellular metabolism and can also ultimately lead to cell death.

Hydroperoxides are known to cause oxidative stress and toxicity in various tissues (Bellomo et al., 1982a; Smith et al., 1984). They are metabolized by the glutathione peroxidase system (Lotscher et al., 1979) and can induce the oxidation of pyridine nucleotides (Lehninger et al., 1978; Lotscher et al., 1979). In addition, other forms of cell injury induced by oxidative stress include those characterized by specific cell surface alterations (Bellomo et al., 1982b; Jewell et al., 1982). In these studies, the organic hydroperoxide t-butylhydroperoxide (t-BHP) was utilized as a model to examine the effects of oxidative stress on mitochondrial function (Sies, 1985; Kennedy et al., 1992). In fact, t-BHP has been shown to specifically alter different mitochondrial regulatory mechanisms and to modulate both mitochondrial (NADPH-dependent) and extramitochondrial (thiol-dependent) calcium compartmentalization and homeostasis (Bellomo and Mirabelli, 1992; Van Den Berg et al., 1992).

The aim of the present study was to determine the *in vitro* effects of the oxidizing agent t-BHP on different human cell lines having different histotype and growth features by using electron microscopy and electron paramagnetic resonance spectroscopy. The results obtained seem to indicate that, depending upon the cell type, the cytoskeleton as well as mitochondria can represent primary targets of t-BHP. In addition, the cells with stronger cell–substratum interactions appear to be less susceptible to t-BHP-mediated cell death. In particular, epithelial A431 cells, which grow in monolayer, are the least susceptible, while U937 leukemia cells, which grow in suspension, are the most susceptible.

Methods

Cell cultures

A431 cells, a human epidermoid carcinoma cell line, were grown in DMEM, while ADF, a human astrocytoma, and U937, a monocytic cell line, were grown in RPMI 1640. All cultures were grown at 37°C and supplemented with 10% fetal calf serum (Flow Laboratories, Irvine, UK), 1% nonessential amino acids, 5 mmol/L L-glutamine, penicillin (100 IU/ml) and streptomycin (100 µg/ml). For light and scanning microscopy, both control and treated cells adhering to the substrate (A431 and ADF) were grown on 13-mm-diameter glass coverslips in separate wells (5×10^4 cells/well). Control and treated U937 cells, which grow in suspension, were collected by centrifugation and the pellets were allowed to adhere onto polylysine-coated glass coverslips. For transmission electron microscopy, cells were subcultured in 25-cm^2 Falcon plastic flasks at a density of approximately 10^5 cells/ml. Flasks and wells were placed in a 37°C incubator containing an atmosphere of 95% air and 5% CO_2. For electron paramagnetic resonance analyses, A431 and ADF cells were removed by rubber policeman, centrifuged for 5 min at 800 rpm and resuspended in phosphate-buffered saline (PBS, pH 7.4). U937 cells were collected directly by centrifugation for 5 min at 800 rpm and also resuspended in PBS.

Cell treatments

Twenty-four hours after seeding, cell cultures were treated, by direct addition to the culture medium, with 3.0 mmol/L t-BHP for 30, 60, 90, or 120 min. In order to evaluate cell viability after t-BHP exposure, the trypan blue dye exclusion test was performed.

Scanning electron microscopy

Control and treated cells were washed in PBS and fixed with 2.5% glutaraldehyde in 0.1 mol/L cacodylate buffer (pH 7.4) containing 3% w/v sucrose at room temperature for 20 min. Following postfixation in 1% osmium tetroxide

for 30 min, cells were dehydrated through graded ethanols, critical point dried in CO_2, and gold coated by sputtering. The samples were examined with a Cambridge 360 scanning electron microscope.

Cytoskeleton analysis

Cells were fixed with 3.7% formaldehyde in PBS (pH 7.4) for 10 min at room temperature. After washing in the same buffer, the cells were permeabilized with 0.5% Triton X-100 (Sigma) in PBS for 5 min at room temperature. Cells were stained with fluorescein–phalloidin (Sigma) or with a mixture of α and β (1:1) anti-tubulin antibodies (Sigma) at 37°C for 30 min. For the detection of tubulin, cells were then incubated with anti-rabbit IgG-fluorescein-linked whole antibody (Amersham International) at 37°C for 30 min. Finally, after washing, all the samples were mounted with glycerol–PBS (1:1) and observed with a Nikon Microphot fluorescence microscope.

Transmission electron microscopy

For ultrathin sectioning, cells were fixed with 2.5% glutaraldehyde in 0.1 mol/L cacodylate buffer (pH 7.3), postfixed with 1% osmium tetroxide in the same buffer for 1 h, dehydrated through graded ethanols, and embedded in Agar 100 resin (Agar Aids, Stansted, Essex, UK). Ultrathin sections, obtained with an LKB ultramicrotome (Ultratome Nova), were stained with uranyl acetate and lead citrate. Finally, sections were observed with a Zeiss EM10C electron microscope.

Determination of GSH

Considering the role of endocellular free-radical production and in order to obtain information about the redox state of cells treated with t-BHP, intracellular GSH level was measured as acid-soluble thiols using a colorimetric assay (Saville, 1958).

EPR measurements

About 2×10^6 cells for each type of control and treated cells were collected by centrifugation and resuspended in PBS (0.5 ml). The cells were labeled with a solution of 5-nitroxystearate (5-NSA) (Aldrich Chemical Co., Milwaukee,, WI, USA) in absolute ethanol to a final nitroxystearate concentration of 50 μmol/L (Santini et al., 1987). The cell suspension was gently vortexed, incubated for 2 min at room temperature and aspirated into Teflon gas-permeable tubing (Zeus Industrial Products, Inc., Raritan, NJ, USA) via syringe. The tubing was then placed in an open-ended quartz capillary tube. EPR measurements were carried out on a temperature-controlled Varian X-band spectrometer with a liquid air gas flow. This flow allowed oxygenation of the cells throughout spectra acquisition. The EPR spectrometer was operated at a microwave frequency of 9.12 GHz, at a power of 10 mW, a field modulation of 100 kHz, a modulation amplitude of 2 G and a time constant of 1 s. Temperature was monitored by digital thermometer with its thermocouple inserted into the capillary tube holder, and temperature was maintained to within ± 0.5°C. About two minutes were allowed for temperature equilibration between each temperature measured. EPR spectra were recorded at temperatures between 15°C and 37°C and membrane order was calculated at these different temperatures so as to have a more complete analysis of membrane behavior and because more subtle changes in membrane structure can be detected over a range of temperatures. Samples from at least five separate experiments for control and t-BHP-treated cells were examined. For all temperature values, the distance between the

outer hyperfine splitting ($2T_{\parallel}'$) was measured directly from the spectra and used as an indicator of membrane order. After obtaining a full scan, the gain was increased tenfold in order to measure the splitting more accurately. The parameters that contribute to EPR spectra of cell membranes are not fully understood but they include mobility of phospholipids in the bilayer, local changes in charge across the membrane, and molecular ordering. While we have referred to changes in $2T_{\parallel}'$ as changes in membrane order, $2T_{\parallel}'$ should be understood as an empirical measure of molecular motion in the immediate vicinity of the spin-label probe. For a complete theoretical treatment of the use of spin labels in membranes, see McConnell and Gaffney McFarland (1970).

Results

Morphological analyses

First, the three cultured cell lines different in histotype, growth features and morphology were analyzed by light microscopy and scanning electron microscopy (SEM). Epidermoid carcinoma A431 control cells appeared as flat polygonal-shaped epithelial cells (Figure 1a) while most ADF astrocytoma control cells were bipolar in nature (Figure 1c). Cell morphology changes induced by t-BHP were followed by inverted microscopy in all the cell types considered here. The progressive retraction of the cell body and cell rounding were in fact easily appreciable in A431 and ADF cells after short-time treatment with 3 mmol/L t-BHP. However, the variations were induced after different exposure times and appeared to be different in extent. Accordingly, an extensive SEM analysis was carried out. Important massive modifications, e.g., of cell-to-cell and cell–substratum contacts were observed after 120 min in A431 cells (Figure 1b). In addition, the formation of surface protrusions or blebs, a well-known marker of cellular damage, was also detected. However, in A431 cells, the blebs were small and blebbing was limited to only a few cells (Figure 1b). In contrast, a higher susceptibility was appreciated by SEM observations in ADF cells. Surface changes including microvillar rearrangement, retraction of the cell body, cell rounding and the formation of surface protrusions were detected after 90 min of 3 mmol/L t-BHP exposure. It is also interesting to note that the blebs were collapsed in nature (Figure 1d). Finally, U937 cells were also studied in order to determine whether these cells growing in suspension, and not in monolayer, could undergo changes similar to those described above. In fact, alterations of normal surface structure of U937 cells shown in Figure 2a were detected after 15 min of exposure to t-BHP (Figure 2b). Lamellar surface structure present in control cells was modified, small blebs were formed, and microvillar organization was altered (Figure 2b). In order to investigate further the effects of t-BHP on U937 cells, a time course of the morphological alterations was also conducted. After 30 min of exposure, microvillous structures were shortened, swollen or completely disrupted (Figure 2c). Finally, after 90 min, multiple blebbing was present in nearly all the cells. In addition, the blebs in these cells are elongated, aligned, interconnected, and not collapsed as in ADF cells (Figure 2d, 'serial' blebbing, arrow). When a quantitative evaluation was conducted of the damage induced after t-BHP treatment in all the cell types studied here, the results summarized in Figure 3 emerged. As can be seen, these cells have different susceptibilities to both bleb formation and cell death after 1 h treatment with t-BHP. A431 cells, which have the strongest cell-to-cell contacts of the cells examined here, appeared to be the most resistant to damage and death induced by this substance, while U937 cells, which grow in suspension, are the most susceptible.

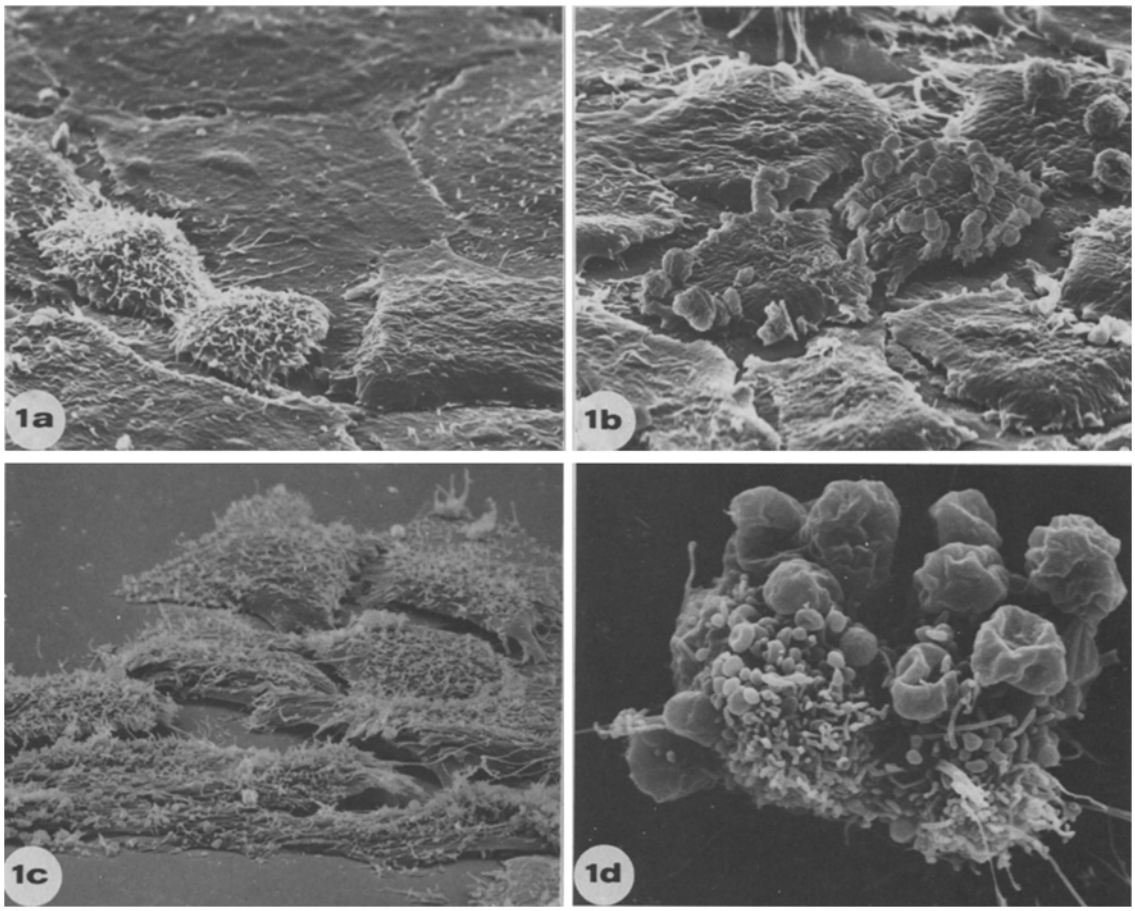

Figure 1. Scanning electron micrographs of (a) A431 control cells, (b) A431 cells treated with 3 mmol/L t-BHP for 120 min, (c) ADF control cells and (d) ADF cells treated with 3 mmol/L t-BHP for 90 min. Control flat and adhering A431 cells (a) undergo retraction and blebbing after t-BHP exposure (b). In ADF cells, the presence of numerous collapsed blebs is also visible (d).

Subcellular element analysis

Cytoskeleton

Because of the well known effects of oxidative stress on subcellular components and in consideration of the target effect of some oxidizing agents on cytoskeletal elements (Bellomo and Mirabelli, 1990), a fluorescence microscopic evaluation of actin and tubulin organization in control and A431 cells treated with t-BHP for 1 h was conducted. These cells, which grow in monolayer and have a well-developed cytoskeleton, were chosen as an example of the possible changes occurring in this subcellular structure following t-BHP exposure (Figure 4). As can be seen in Figure 4a, A431 control cells have a characteristic distribution of the microfilament network, with numerous filaments distributed in the cell periphery. In addition, the normal polygonal shape of A431 cells and the extensive contact zones between cells are also visible. After 1 h treatment with t-BHP, a time-dependent alteration of the actin filament network was detected in these cells. In fact, with respect to control cells, a progressive collapse and derangement of actin microfilament assembly

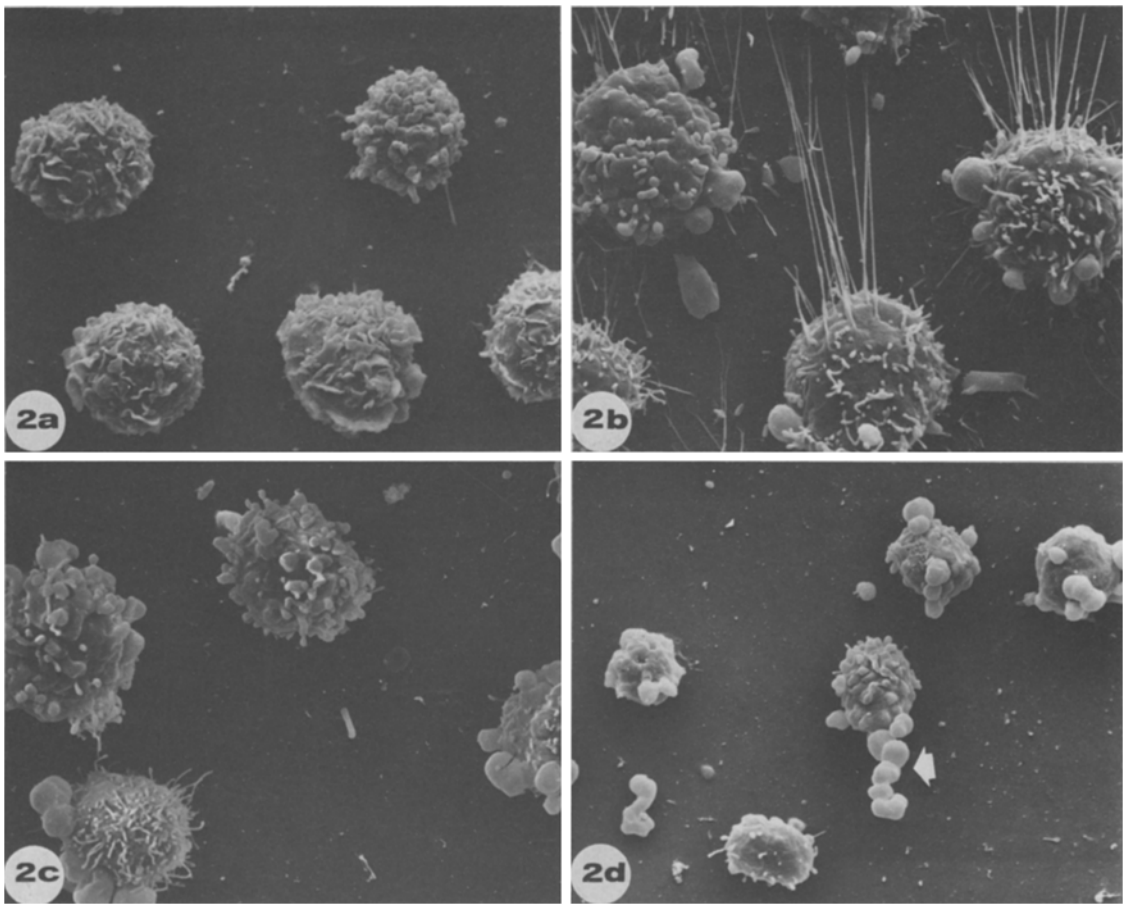

Figure 2. Scanning electron micrographs of (a) U937 control cells, (b) U937 cells treated with 3 mmol/L t-BHP for 15 min, (c) U937 cells treated with 3 mmol/L t-BHP for 30 min and (d) U937 cells treated with 3 mmol/L t-BHP for 90 min. Different alterations can be observed on the cell surface of this cell type: early changes are represented by a marked increase of microvillar structures (b); late modifications are represented by multiple (c) as well as characteristic 'serial' blebbing, i.e., the formation of blebs over other previously formed blebs (d, arrow).

was detected (Figure 4b). In contrast, the microtubule network, shown in Figure 4c, was only partially altered by a 1 h t-BHP exposure (Figure 4d).

Subcellular organelles

In order to evaluate t-BHP-induced subcellular damage more accurately, transmission electron microscopy was conducted on ADF and A431 control cells and these cells treated with the hydroperoxide (Figure 5). Figure 5a shows normal mitochondrial structure in control ADF cells: the electron-dense matrix and regular cristae distribution were observed. After 90 min of t-BHP exposure (Figure 5b), surface blebs were clearly evident and no cellular organelles were present in them. In fact, only ribosomes, well distributed in the bleb matrix, were visible. Thus, these blebs can be classified as potocytotic (Coakley, 1987). In addition, the membrane surrounding the blebs shows numerous invaginations, supporting the SEM

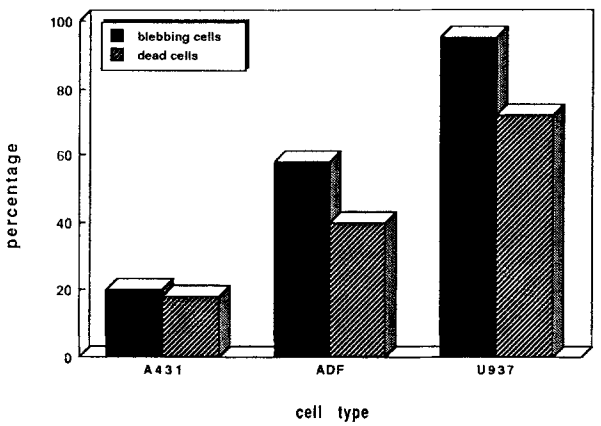

Figure 3. Histogram representing percentage of blebbing and dead A431, ADF and U937 cells after 1 h t-BHP treatment. Percentage blebbing was obtained by counting at least 300 cells in a random manner. Percentage dead cells was determined by the trypan blue exclusion test. All experiments were repeated at least 3 times. Variations between each experiment were less than 10%.

observations of collapsed blebs. In parallel with these important surface modifications after 90 min of treatment, mitochondrial and ER structure was apparently modified (Figure 5c): the mitochondrial matrix was rarefied and cristae were distorted. In contrast, treatment of A431 cells with t-BHP for 1 and 2 h resulted in massive mitochondrial damage. After 1 h treatment (Figure 5e), a slight mitochondrial swelling was appreciable and cristae appeared to be partially distorted and disrupted with respect to controls (Figure 5d). After 2 h exposure (Figure 5f), the mitochondria appeared to be remarkably swollen, the matrix completely rarefied and the cristae disrupted. It should be noted that although mitochondria were altered in both A431 and ADF cells, the damage was particularly marked in A431 cells, in which the progression of mitochondrial lesions was more rapidly induced by t-BHP.

Intracellular GSH levels

In view of the ability of t-BHP to induce oxidative stress in cells, and considering the role of GSH as the most important endocellular defense against oxidative damage, a specific analysis of intracellular soluble thiols, as an indirect measure of reduced glutathione, was carried out in the cultured cells. The results obtained using 3 mmol/L t-BHP demonstrated a remarkable depletion (67% with respect to control values) of GSH content after 30 min of exposure to the hydroperoxide in ADF cells (Figure 6). Treatment for more extended periods (up to 120 min) showed a continued but significantly minor loss of this thiol compound. Slightly different values were obtained in other cell lines used. However, the trend of the curve when expressed in terms of percentage with respect to time zero was apparently the same (not shown). Statistical analyses were conducted on the data obtained from five separate experiments using Student's *t*-test. The variation in values obtained in the same cell group was less than 10%, and a significant difference was obtained ($p<0.001$) between control and treated cell groups.

Biophysical studies

In Figure 7 is shown membrane order (as measured by $2T_{\parallel}'$) as a function of temperature of control A431 cells and A431 cells treated with 3 mmol/L t-BHP for 1 and 2 h. As can be seen, all cells treated with t-BHP have a higher membrane order ('rigidity') than control cells, indicating that this compound induces important variations in the membranes of the treated cells. It should also be noted that there are no significant differences in membrane order between cells exposed to t-BHP for different lengths of time.

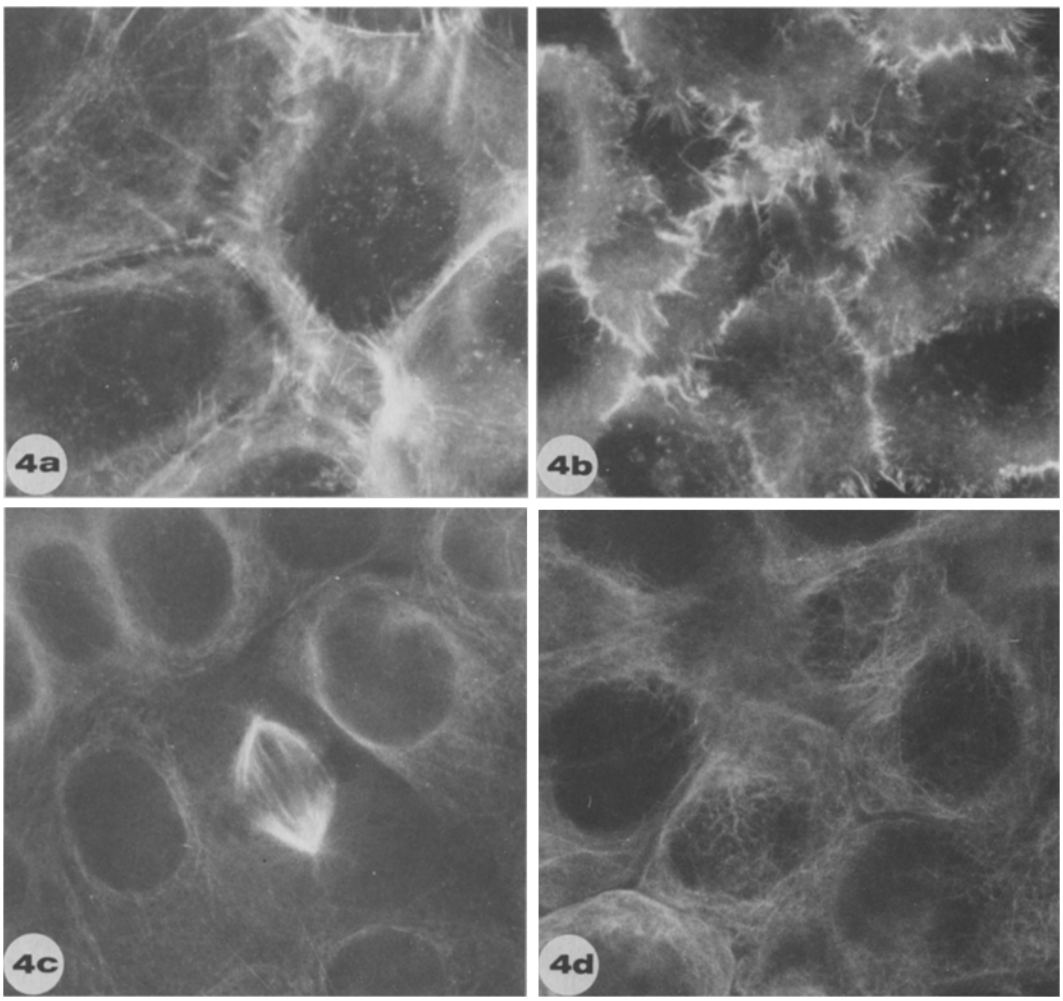

Figure 4. Fluorescence staining with fluorescein–phalloidin of (a) control and (b) 1 h, 3 mmol/L t-BHP-treated A431 cells. Immunostaining with anti-α,β-tubulin of control (c) and 1 h, 3 mmol/L t-BHP-treated A431 cells (d). The remarkable rearrangement of cytoskeletal structures is evident.

Discussion

The data reported here demonstrate that cell structure and function can be affected by t-BHP-mediated oxidative stress by a mechanism involving two subcellular compartments: the mitochondria and the cytoskeleton. However, the primary target effect of t-BHP appears to depend upon the cell histotype. The first, primary lesion was in fact localized in the mitochondria of epithelial A431 cells, which, before undergoing death, show important morphological changes and surface blebbing only after prolonged t-BHP exposure. In contrast, these critical surface alterations occurred rapidly and led to cell lysis in the astrocytic cell type ADF or in myelomonocytic U937 cultured cells before the mitochondria were affected. As a consequence, cell death processes occurred rapidly in these cell types. These results provide new insights into the previously hypothesized mechanisms of t-BHP cytotoxicity and suggest that mitochondrial damage could also play a minor role in hydroperoxide damage.

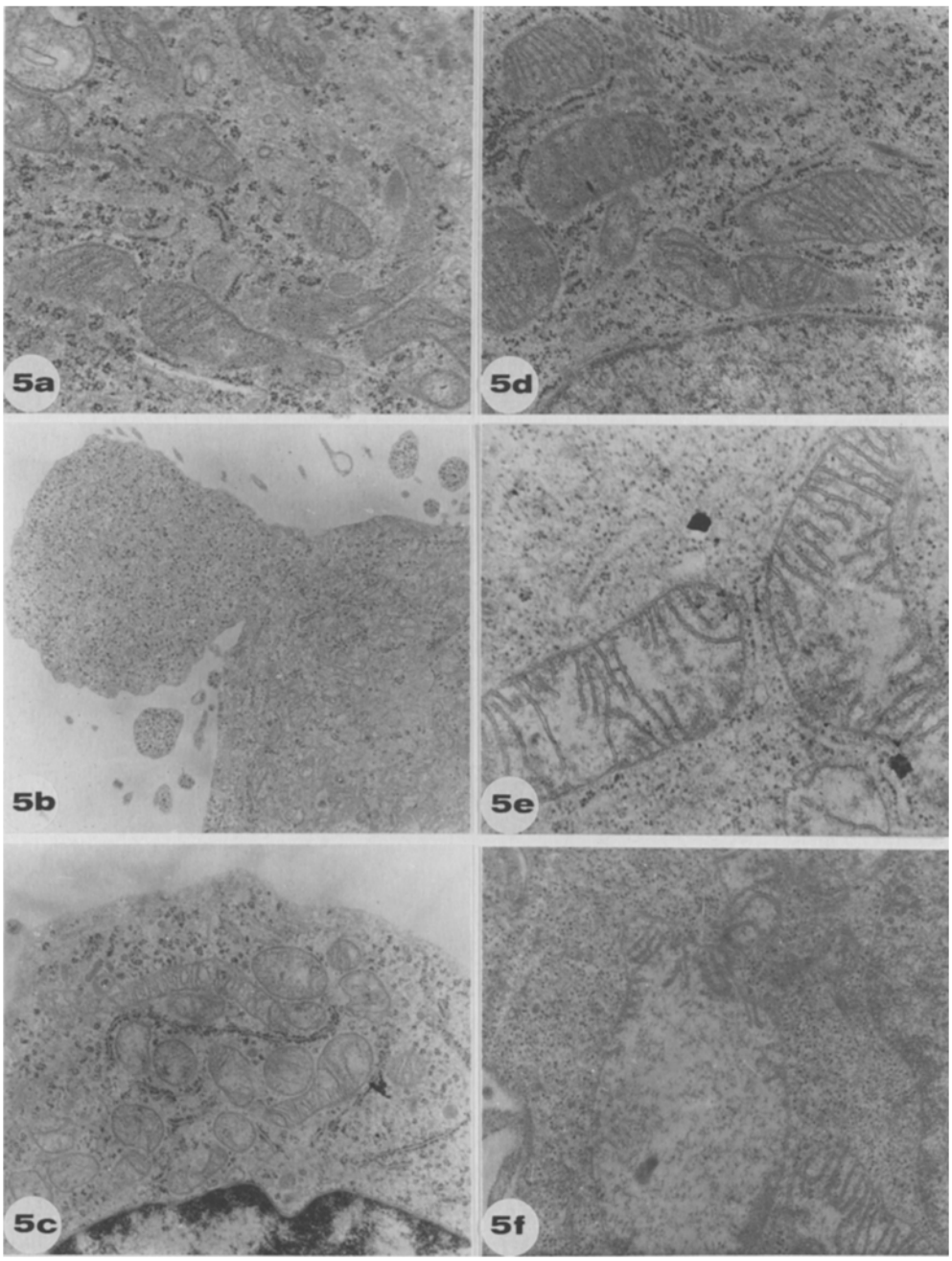

Figure 5. Transmission electron micrographs of ADF (left column) and A431 (right column) cells: (a) control ADF cells, (b) control A431 cells, (c) ADF cells exposed to 3 mmol/L t-BHP for 90 min, (d) A431 cells exposed to 3 mmol/L t-BHP for 60 min, (e) ADF cells exposed to 3 mmol/L t-BHP for 90 min, (f) A431 cells exposed to 3 mmol/L t-BHP for 120 min. Surface blebs characterized by the absence of organelles inside their cytoplasm (potocytosis) are induced by t-BHP (c). Mitochondrial alterations in this cell type are shown in (e). In A431 cells, mitochondrial lesions increase remarkably upon exposure to the oxidizing agent and are characterized by a progressive rarefaction of the matrix and a distortion of the cristae (d), resulting ultimately in complete extraction of the former and the disruption of the latter (f). Note that mitochondrial lesions occur more rapidly in ADF cells than in A431 cells.

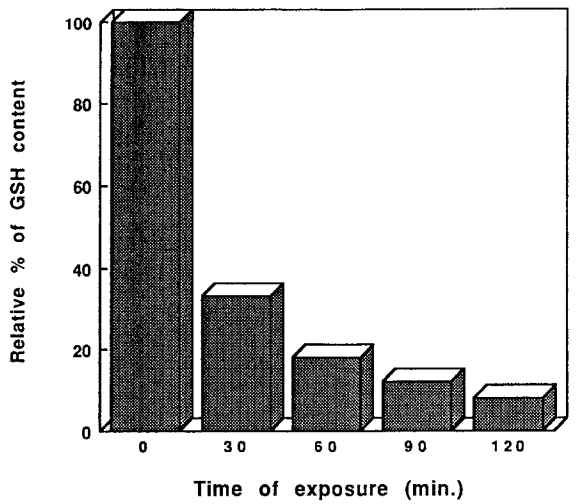

Figure 6. Evaluation of GSH content in control and 3 mmol/L t-BHP-treated ADF cells at 30, 60, 90, and 120 min. At least 3 separate experiments were conducted. Variations between each experiment were less than 10%. Results are expressed as percentage of control (time zero), which is considered as 100%.

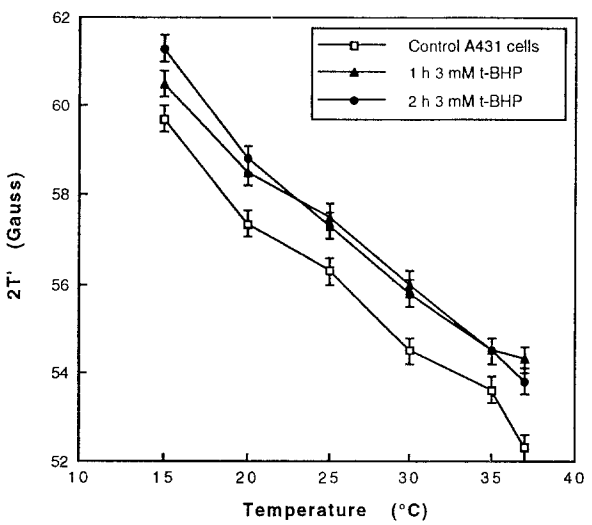

Figure 7. Membrane order (as measured by 2T') as a function of temperature of control A431 cells and A431 cells treated with 3 mmol/L t-BHP for 1 and 2 h. As can be seen, there is an increase in membrane order ('rigidity') as a function of temperature as well as a higher membrane order in cells treated with t-BHP. The means and standard deviations from 4 separate experiments are shown.

In particular, the mechanism of t-BHP-induced cytotoxicity seems to be associated to the different growth features and adhesion properties of cells. In fact, the general morphological features distinguishing the cultured cells considered here are represented mainly by differences in cell-to-cell and cell–substrate relationships. These features appear to be critical in determining different cell susceptibilities to oxidative stress. The results obtained also seem to indicate that cell survival was lower the weaker was cell adhesion. In fact, U937 cells growing in suspension are the most susceptible to t-BHP-mediated stress. In addition, when cultured cells developed large areas of adherence to the substrate, formed desmosomes and displayed a well-organized cytoskeletal network, e.g., in A431 epithelial cells, cell death occurred much later. Hence, in view of the well established importance of the extracellular matrix of adhesion molecules and of the precise relationships occurring between such molecules and the cytoskeleton (Hynes, 1992; Luna and Hitt, 1992), t-BHP appears to exert its intracellular effects by affecting cytoskeleton network integrity and function.

The data reported here seem to suggest that cytoskeletal elements could represent important targets of t-BHP-mediated oxidative stress and that this change can lead to changes in cell ionic homeostasis and viability. In particular, the junction sites between different cytoskeletal elements can be hypothesized to be affected by t-BHP (Malorni et al., 1993). The denaturating activity of t-BHP on cytoskeleton assembly can be associated with a specific cell injury process, i.e., multiple surface blebbing, and to the loss of plasma membrane integrity and cell viability (Orrenius et al., 1989). This hypothesis, previously demonstrated in other experimental situations (Bellomo and Mirabelli, 1992; Malorni et al., 1991), is supported by the biophysical changes, i.e., increase in membrane order, found in the membranes of A431 cells after treatment with t-BHP. This increase in membrane order may be associated to the peroxidation of membrane lipids, which is known to occur in complex systems and is very similar in all the cultured cells considered here.

Thus, it is very likely that this subcellular structure could not play a primary role in t-BHP-mediated injury in all cell types.

However, the effect of t-BHP on cell membranes, including mitochondrial membrane, represents a constant finding that accompanies the process leading to necrotic cell death (Duncan and Shamsadeen, 1993). The occurrence of t-BHP-mediated mitochondrial lesions has been ascribed to specific radical and nonradical pathways (Kennedy et al., 1992) and changes in ionic homeostasis have also been detected in diverse cell systems (Imberti et al., 1993). Incomplete removal of water-soluble hydroperoxides such as hydrogen peroxide will thus result in increased radical formation, leading to oxidative damage in the membrane compartment or in the cytosol. With this in mind, we can hypothesize that alterations of the redox state of certain molecules, e.g., of the cytoskeleton, changes in ionic balance, together with a direct effect on key membranes, such as the inner mitochondrial membrane or plasma membrane, can lead to cell lysis. The process could occur by the cytoskeleton-dependent cascade of alterations in these cell hystotypes characterized by a 'susceptible', poorly developed cytoskeletal network. In contrast, when cell adhesion was particularly strong and stable, typical mitochondrial-lesion-mediated cell death could occur. In conclusion, this paper seems to suggest that hydroperoxide damage can affect both cell membrane and cytoskeletal elements, probably through different radical species capable of modifying specific sites on certain molecules, or junction sites, which play an important role in cell integrity and viability.

References

Bellomo G, Mirabelli F. Oxidative stress and cytoskeletal alterations. Ann NY Acad Sci. 1992;663:97–109.

Bellomo G, Jewell SA, Thor H, Orrenius S. Regulation of intracellular calcium compartmentation: studies with isolated hepatocytes and t-butyl hydroperoxide. Proc Natl Acad Sci USA. 1982a;79:6842–6.

Bellomo G, Jewell SA, Orrenius S. The metabolism of menadione impairs the ability of rat liver mitochondria to take up and retain calcium. J Biol Chem. 1982b;257:11558–62.

Coakley WT. Hyperthermia effects on the cytoskeleton and on cell morphology. In; Bowler K, Fuller BJ, eds. Temperature and animal cells. Cambridge: Company of Biologists Ltd; 1987:187–211.

Duncan CJ, Shamsadeen N. Ultrastructural changes in mitochondria during rapid damage triggered by calcium. In: Duncan CJ, ed. Calcium, oxygen radicals and cellular damage. Cambridge: Cambridge University Press; 1993:149–64.

Hynes RO. Integrins: versatility, modulation, and signalling in cell adhesion. Cell. 1992;69:11–25.

Imberti R, Nieminen AL, Herman B, Lemasters JJ. Mitochondrial and glycolytic dysfunction in lethal injury to hepatocytes by t-butylhydroperoxide: protection by fructose, cyclosporin A and trifluoperazine. J Pharmacol Exp Ther. 1993;265:392–400.

Gutteridge JMC. Free radicals in disease processes: a compilation of cause and consequence. Free Rad Res Commun. 1993;19:141–58.

Jewell SA, Bellomo G, Thor H, Orrenius S, Smith MT. Bleb formation in hepatocytes during drug metabolism is associated with alterations in intracellular thiol and calcium ion homeotasis. Science. 1982;217:1257–9.

Kennedy CH, Church DF, Winston GW, Pryor WA. tert-Butyl hyperoxide-induced radical production in rat liver mitochondria. Free Rad Biol Med. 1992;12:381–7.

Lehningher AL, Vercesi AE, Bababunmi EA. Regulation of Ca^{2+} release from mitochondria by the oxidation reduction state of pyridine nucleotides. Proc Natl Acad Sci USA. 1978;75:1690–4.

Lotscher HR, Winterhalter KH, Carafoli E, Richter C. Hydroperoxides can modulate the redox state of pyridine nucleotides and calcium balance in rat liver mitochondria. Proc Natl Acad Sci USA. 1979;76:4340–4.

Luna EJ, Hitt AL. Cytoskeleton-plasma membrane interactions. Science. 1992;258:955–64.

Malorni W, Iosi F, Marabelli F, Bellomo G. Cytoskeleton as target in menadione-induced oxidative stress in cultured mammalian cells: alterations underlying surface bleb formation. Chem Biol Interact. 1991;80:217–36.

Malorni W, Iosi F, Donelli G, Caprari P, Salvati AM, Cianciulli P. A new striking morphologic feature for the human erythrocyte in hereditary spherocytosis: the blebbing pattern. Blood. 1993;81:2821–2.

McConnell HM, Gaffney McFarland B. Cytochalasin B disrupts the association of filamentous web and plasma membrane in hepatocytes. Q Rev Biophys. 1970;3:91–136.

Orrenius S, McConkey DJ, Bellomo G, Nicotera P. Role of calcium in toxic cell killing. Trends Pharm Sci. 1989;10:281–5.

Santini MT, Indovina PL, Hausman RE. Changes in myoblast membrane order during differentiation as measured by EPR. Biochim Biophys Acta. 1987;896:19–25.

Saville B. A scheme for the colorimetric determination of microgram amounts of thiols. Analyst. 1958;83:670–2.

Sies H. Oxidative stress: introductory remarks. In: Sies H, ed. Oxidative stress. London: Academic Press; 1985:1–8.

Sies H. Oxidative stress: from basic research to clinical application. Am J Med. 1991;91(3C):31–8.

Smith MT, Thor H, Jewell SA, Bellomo G, Sandy MS, Orrenius S. Free radical-induced changes in the surface morphology of isolated hepatocytes. In: Armstrong D, et al. Free radicals in molecular biology, aging and disease. New York: Raven Press; 1984:103–18.

Van Den Berg JJM, Op den Kamp JAF, Bertram HL, Roelofsen B, Kuypers FA. Kinetics and site specificity of hydroperoxide-induced oxidative damage in red blood cells. Free Rad Biol Med. 1992;12:487–98.

Address for correspondence: Dr Walter Malorni, Department of Ultrastructures, Istituto Superiore di Sanità, Viale Regina Elena 299, 00161 Rome, Italy